The Journal of Chemical Physics

Multiple time scale open systems: Reaction rates and quantum coherence in model retinal photoisomerization under incoherent excitation

Cite as: J. Chem. Phys. **151**, 014104 (2019); https://doi.org/10.1063/1.5099969
Submitted: 13 April 2019 • Accepted: 07 June 2019 • Published Online: 02 July 2019

Simon Axelrod and Paul Brumer

The Journal of Chemical Physics ARTICLE scitation.org/journal/jcp

Multiple time scale open systems: Reaction rates and quantum coherence in model retinal photoisomerization under incoherent excitation

Cite as: J. Chem. Phys. 151, 014104 (2019); doi: 10.1063/1.5099969
Submitted: 13 April 2019 • Accepted: 7 June 2019 •
Published Online: 2 July 2019

Simon Axelrod and Paul Brumer[a)]

AFFILIATIONS

Chemical Physics Theory Group, Department of Chemistry, and Centre for Quantum Information and Quantum Control, University of Toronto, Toronto, Ontario M5S 3H6, Canada

Note: This paper is part of a JCP Special Topic on Dynamics of Open Quantum Systems.
[a)]**Electronic mail:** paul.brumer@utoronto.ca

ABSTRACT

Many important open quantum systems, such as light harvesting systems irradiated with natural incoherent light, present challenging computational problems. Specifically, such systems are characterized by multiple time scales over many orders of magnitude. We describe and apply an efficient approach to determine rates and dynamics in such systems. As an example, we present a theoretical and computational analysis of retinal isomerization under incoherent solar excitation using a minimal retinal model. Solar- and bath-induced Fano coherences are shown to have a small but non-negligible effect on the reaction dynamics, and the effect of Fano coherences on the reaction rate is shown to depend strongly upon the form and strength of the system-bath coupling. Using the isomerization probability to obtain the time-dependent cellular hyperpolarization, we show that the effect of coherence on hyperpolarization dynamics is small compared to the effect of natural variations in the solar intensity.

I. INTRODUCTION

The extent to which quantum mechanics is necessary to understand biological processes is a question of considerable interest in the scientific community and of particular relevance in the area of open quantum systems. The relevance of quantum effects such as entanglement and quantum coherence has been considered in the context of both photosynthesis[1–6] and photoisomerization.[7–9] For example, pulsed laser experiments have explored the role of quantum coherence (off-diagonal elements of the density matrix in the energy basis) in the *cis-trans* isomerization of retinal in rhodopsin.[7–9] This ubiquitous process is a key component of, e.g., vision,[10] light-sensing,[11] and bacterial proton pumping.[12] Understanding the physical principles that underlie photoisomerization thus has widespread implications in biology. Utilizing similar principles may also contribute to the design of efficient photovoltaics[13–15] and single photon detectors.[16–18] It is therefore of interest to explore the role of coherence in the photoisomerization of retinal.

The observation of *oscillating* coherences in the 2D photon echo spectroscopy of such systems is a consequence of pulsed laser excitation,[19–21] whereas the generation of *stationary* coherences can occur under natural incoherent light.[22,23] Indeed, natural conditions involve incoherent (e.g., solar) excitation (coupling to a "hot bath"), as well as environment-induced dephasing and nonradiative decay (coupling to a "cold bath"). Therefore, a description of such systems under natural conditions requires an open quantum system treatment. In Ref. 24, a Redfield master equation was used to examine coherences in model retinal. Its effect on the quantum yield over a *picosecond time scale* was analyzed and found to be small. However, it is also important to examine these systems on longer time scales relevant to biological processes (i.e., milliseconds). A computational study of this kind can be time-consuming due to the small time step needed to follow the underlying fast molecular dynamics and hence solve the master equation. For this reason, we recently introduced a more efficient computational approach to the long-time dynamics under natural incoherent excitation conditions such as sunlight or noise.[25]

In this work, we utilize this recently developed methodology[25] to explore the effect of coherence on the reaction rate of retinal isomerization. Isomerization is modeled using a two state, two mode model for retinal[26] that reproduces important ultrafast spectroscopic isomerization features. We demonstrate that coherence can be associated with a small but nonnegligible change in the isomerization dynamics over biological time scales. The effect of stationary coherence on the reaction rate is shown to depend strongly on the strength and form of the system-bath coupling. In this regard, we note our ongoing efforts to improve the widely used retinal model employed in this study.[27]

This paper is organized as follows: In Sec. II, we review the theoretical framework introduced in Ref. 25 to reconstruct quantum mechanical reaction dynamics and describe a minimal model for retinal isomerization. In Sec. III, we present the results for model retinal in rhodopsin and analyze the role of coherence in the isomerization process. In Sec. IV, we summarize the results and discuss their significance.

II. THEORY: REACTION DYNAMICS

A. Reconstruction of molecular dynamics

Simulating the long time dynamics of retinal isomerization under natural weak excitation is challenging, since the excitation is significantly slower than internal relaxation.[24,28] This precludes the possibility of coarse-graining the system dynamics on the excitation time scale. Motivated by these considerations, we recently developed a method of reconstructing quantum dynamics without a direct solution to the quantum master equation.[25] The methodology is generally applicable to multitime scale problems. Below, we review this approach and its computational advantages.

To follow the dynamics, focus on a general operator $\hat{O}$ that monitors a physical process. As an example, consider a reaction of the form $R \rightleftharpoons P$, where R denotes the reactant, P denotes the product, and $\hat{R}$ and $\hat{P}$ are the associated projection operators onto reactant and product species. Then, an operator of interest could be $\hat{O} = \hat{R}$ or $\hat{O} = \hat{P}$ with the expectation value $\langle \hat{O}(t) \rangle = \mathrm{Tr}[\hat{\rho}(t)\hat{O}]$, where $\hat{\rho}(t)$ is the density operator in the Schrödinger picture. Here, $\langle \hat{O}(t) \rangle$ is then reconstructed through projection onto an exponential basis set,

$$\langle \hat{O}(t) \rangle = \mathrm{Tr}[\hat{\rho}_s \hat{O}] + \sum_m f_m e^{-k_m t}, \tag{1}$$

where $\hat{\rho}_s = \hat{\rho}(t \to \infty)$ is the steady-state density operator, the f_m are weight functions, and the k_m are real decay rates. If one can obtain $\hat{\rho}_s$, the weights f_m, and the decay rates k_m, then one can monitor the process of interest over long time scales without integrating a quantum master equation. If the f_m and k_m can be calculated more rapidly than integrating a master equation, then the method is more efficient than solving a master equation.

One way to calculate the f_m and k_m is from a set of "progress moments" I_n, defined by

$$I_n = \int_0^\infty dt\, t^n (\langle \hat{O}(t) \rangle - \mathrm{Tr}[\hat{\rho}_s \hat{O}]), \tag{2}$$

with n being a non-negative integer. Here, the time $t = 0$ defines the start of the dynamics; for example, in light-induced processes, it is the time at which the molecule and solar radiation first interact. (An alternative method involves Laplace transforms.[25]) Inserting Eq. (1) into Eq. (2) gives

$$\sum_m f_m (k_m)^{-n} = \begin{cases} \langle \hat{O}(t=0) \rangle - \mathrm{Tr}[\hat{\rho}_s \hat{O}], & \text{if } n = 0, \\ I_{n-1}/(n-1)! & \text{if } n \neq 0. \end{cases} \tag{3}$$

Given $\hat{\rho}_s$ and the I_n, one can then obtain the f_m and k_m through Eq. (3) and hence reconstruct $\langle \hat{O} \rangle$ through Eq. (1). Note that the number of required basis functions is especially small when $\langle \hat{O}(t) \rangle$ is approximately exponential. Further details of the solution of Eq. (3) are provided in Ref. 25.

To obtain the I_n, note that $I_n = \mathrm{Tr}[\delta\hat{\rho}_n(\hat{O})]$, where $\delta\hat{\rho}_n = \int_0^\infty dt\, t^n (\hat{\rho}(t) - \hat{\rho}_s)$. To find the operator $\delta\hat{\rho}_n$, consider that in the absence of initial system-environment correlations the density operator evolves according to $\partial_t \hat{\rho}(t) = \int_0^t d\tau\, \hat{\mathcal{K}}(t-\tau)\hat{\rho}(\tau)$,[29–31] where $\hat{\mathcal{K}}(t)$ is the memory kernel. One can then write

$$\hat{0} = \int_0^\infty dt\, t^n \left(-\partial_t [\delta\hat{\rho}(t)] + \int_0^t d\tau\, \hat{\mathcal{K}}(t-\tau)\hat{\rho}(\tau) \right). \tag{4}$$

As shown in Ref. 25, a binomial expansion can be used to rewrite this equation as

$$\hat{0} = \hat{S}_n + \hat{T}_n + \sum_{k=0}^{n} \binom{n}{k} \hat{\mathcal{L}}_{n-k} [\delta\hat{\rho}_k]. \tag{5}$$

Here, $\hat{S}_n = \hat{\rho}_0 - \hat{\rho}_s$ if $n = 0$ and $n \cdot \delta\hat{\rho}_{n-1}$ otherwise, $\hat{\mathcal{L}}_n = \int_0^\infty dt\, t^n \hat{\mathcal{K}}(t)$ [and so $\hat{\mathcal{L}}_0 = \int_0^\infty dt\, \hat{\mathcal{K}}(t)$], $\hat{T}_n = \int_0^\infty dt\, t^n (\int_0^t d\tau\, \hat{\mathcal{K}}(\tau)\hat{\rho}_s)$, and $\binom{n}{k} = n!/[k!(n-k)!]$ is the binomial coefficient. The goal is now to use Eq. (5) to solve for $\delta\hat{\rho}_n$. The quantity $\delta\hat{\rho}_n$ appears in the term $\hat{\mathcal{L}}_0[\delta\hat{\rho}_n]$; one could try to isolate for $\delta\hat{\rho}_n$ by inverting $\hat{\mathcal{L}}_0$. However, $\hat{\mathcal{L}}_0$ is necessarily singular because there exists a nontrivial solution $\hat{\rho}_s$ to the equation $\hat{\mathcal{L}}_0\hat{\rho}_s = \hat{0}$. This implies that $\delta\hat{\rho}_n$ is not uniquely specified by Eq. (5). It is therefore necessary to add more information about $\delta\hat{\rho}_n$ to the equation.

To do so, consider that $\mathrm{Tr}[\delta\hat{\rho}_n] = 0$ since $\mathrm{Tr}[\hat{\rho}(t)] = \mathrm{Tr}[\hat{\rho}_s] = 1$. Specifying the trace of $\delta\hat{\rho}_n$ and requiring it to satisfy Eq. (5) provide enough information to obtain $\delta\hat{\rho}_n$ (see Ref. 25). Since $\mathrm{Tr}[\delta\hat{\rho}_n] = 0$, one can add any quantity proportional to $\mathrm{Tr}[\delta\hat{\rho}_n]$ to the left-hand side of Eq. (5). In particular, one can add $w\hat{\mathcal{T}}[\delta\hat{\rho}_n]$, where w is an arbitrary constant and $\hat{\mathcal{T}}[\hat{O}] \propto \mathrm{Tr}(\hat{O})$ for any operator $\hat{O}$. The superoperator $\hat{\mathcal{T}}$ is defined by its matrix elements $\mathcal{T}_{ijkl} = \delta_{kl}\delta_{ij}\delta_{i1}$ in any basis so that $\hat{\mathcal{T}}[\hat{O}] = \mathrm{Tr}(\hat{O})|1\rangle\langle 1|$. By adding this to the left-hand side of the equation, one obtains

$$-[\hat{\mathcal{L}}_0 + w\hat{\mathcal{T}}]\delta\hat{\rho}_n = \hat{S}_n + \hat{T}_n + \sum_{k=0}^{n-1} \hat{\mathcal{L}}_{n-k}[\delta\hat{\rho}_k]. \tag{6}$$

It can be shown that the operator $[\hat{\mathcal{L}}_0 + w\hat{\mathcal{T}}]$ is nonsingular.[25] Hence, one can isolate for $\delta\hat{\rho}_n$, giving

$$\delta\hat{\rho}_n = -[\hat{\mathcal{L}}_0 + w\hat{\mathcal{T}}]^{-1} \begin{cases} \hat{\rho}_0 - \hat{\rho}_s + \hat{T}_0, & \text{if } n = 0, \\ n \cdot \delta\hat{\rho}_{n-1} + \hat{T}_n + \sum_{k=0}^{n-1} \binom{n}{k} \hat{\mathcal{L}}_{n-k}[\delta\hat{\rho}_k], & \text{if } n \neq 0. \end{cases} \tag{7}$$

These quantum recursive relations [Eq. (7)] are reminiscent of those used to calculate nth passage times in classical barrier crossing problems.[32]

The first few moments of this procedure will produce global long time behavior. The short time details of the reconstructed dynamics may be obtained through the use of an additional Laplace transform, as described in Ref. 25. In the following analysis, the environment is described within a Markovian approximation so that $\hat{T}_n = \hat{0}$ for all n, $\hat{\mathcal{L}}_n = \hat{0}$ for $n \neq 0$, and $\partial_t \hat{\rho}(t) = \hat{\mathcal{L}}_0 \hat{\rho}(t)$.

The goal of reconstructing the system dynamics has therefore been reduced to three steps: first, solve $\hat{\mathcal{L}}\hat{\rho}_s = \hat{0}$ for the stationary state $\hat{\rho}_s$; second, solve Eq. (7) for $\delta\hat{\rho}_n$; and third, solve Eq. (3) for f_m and k_m. The first two steps are the most computationally time consuming. However, as shown in Ref. 25, each of these two calculations can be performed efficiently by using the secular Liouville superoperator as a preconditioner for the full Liouville superoperator. The secular Liouville superoperator is one in which populations and coherences are decoupled through the secular approximation. In this case, the d populations couple to each other, while the evolution of the $d^2 - d$ coherences is known analytically (d is the Hilbert space dimension). Inversion of the $d \times d$ matrix that couples populations can be performed rapidly, and the secular result is a good first approximation to the full nonsecular result. Hence, using the secular Liouville superoperator as a preconditioner allows Eq. (7) to be solved efficiently. The long time system dynamics can hence be obtained rapidly. Below we will apply this method to a model of retinal isomerization and show that it yields a significant enhancement in computational efficiency.

B. Retinal model

Consider now the minimal two-state, two-mode (2S2M) model of retinal in rhodopsin and the master equation that describes coupling to the radiation field and to the "bath" (the protein environment and the unreactive molecular modes). The total system-plus-bath Hamiltonian is given by

$$\hat{H} = \hat{H}_S + \hat{H}_{rad} + \hat{H}_B + \hat{H}_{S-rad} + \hat{H}_{S-B}. \tag{8}$$

Here, $\hat{H}_S$ is the system Hamiltonian, $\hat{H}_{rad}$ is the radiation field Hamiltonian, and $\hat{H}_B$ is the bath Hamiltonian. The last two terms account for the system-environment interaction. The system Hamiltonian is given by the two electronic state, two vibrational mode model,[26,33]

$$\hat{H}_S = \sum_{jj'} \left[\left(\hat{T} + E_j + (-1)^j \frac{1}{2} \tilde{V}_j (1 - \cos\phi) + \frac{1}{2}\omega x^2 + \kappa x \delta_{j,1} \right) \delta_{j,j'} + \lambda x (1 - \delta_{j,j'}) \right] |\psi_j\rangle\langle\psi_{j'}|. \tag{9}$$

Here, x denotes the coordinate of the stretching mode and $\phi \in [-\pi/2, 3\pi/2]$ is the coordinate of the torsional mode. The latter represents the reaction coordinate such that $\phi \in [-\pi/2, \pi/2]$ is associated with the *cis* conformation, and $\phi \in [\pi/2, 3\pi/2]$ is associated with the *trans* conformation.[24] Note that the probability of being in *cis* at time t is $\mathrm{Tr}[\hat{\rho}(t)\hat{P}_{cis}]$, where $\hat{P}_{cis} = \theta(\pi/2 - |\phi|)$, with θ being the Heaviside step function. The kinetic energy is[26] $\hat{T} = -\omega\, \partial_x^2/2 - \partial_\phi^2/2m$, where ω and m^{-1} are energy scales associated with x and ϕ, respectively. The diabatic electronic eigenstates $|\psi_j\rangle = |\psi_0\rangle, |\psi_1\rangle$ have energies E_j and are vibronically coupled through λx. The 2S2M Hamiltonian is characterized by conical intersections at $\phi \approx \pm\pi/2$ and $x = 0$ (see Fig. 1), which play a critical role in retinal isomerization.[34] We use the numerical parameters given in Ref. 26. The potential energy surfaces obtained by diagonalizing the potential energy component of the Hamiltonian (9) are shown in Fig. 1. The 2S2M model reproduces many important aspects of the isomerization process, including the energy storage of the reaction, the high quantum yield, and the transient pump-probe absorption spectrum.[26,33] Improvements to this model are, however, under investigation.[27]

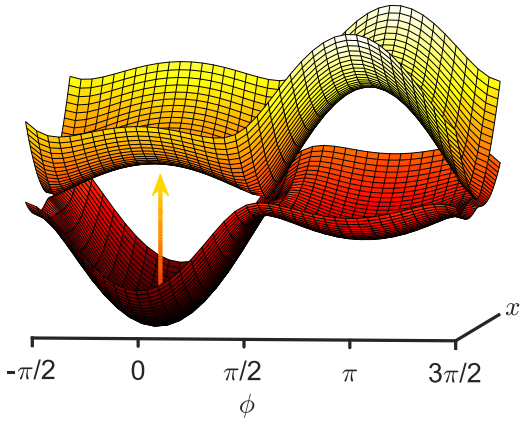

FIG. 1. Potential energy surfaces obtained by diagonalizing the 2S2M retinal Hamiltonian. The two potential energy surfaces cross at conical intersections located at $\phi \approx \pm\pi/2$ and $x = 0$. The *cis* isomer corresponds to $\phi \in [-\pi/2, \pi/2]$, and the *trans* isomer corresponds to $\phi \in [\pi/2, 3\pi/2]$. Incoherent excitation from ground *cis* to excited *cis* is shown with an arrow. Higher energies are shown with a brighter hue.

The radiation field is described by a sum of harmonic oscillators, with $\hat{H}_{rad} = \sum_{\mathbf{k},\lambda} \hbar\omega_k \hat{a}^\dagger_{\mathbf{k},\lambda} \hat{a}_{\mathbf{k},\lambda}$[29] where $\hat{a}^\dagger_{\mathbf{k},\lambda}$ and $\hat{a}_{\mathbf{k},\lambda}$ are the creation and annihilation operators associated with mode k, wave vector $\mathbf{k}$, polarization $\lambda = 1, 2$, and frequency ω_k. The system couples to the incoherent radiation field through an interaction with the dipole vector $\hat{\boldsymbol{\mu}}$ in a cavity of volume $V \to \infty$,[35]

$$\hat{H}_{S-rad} = i\hat{\boldsymbol{\mu}} \cdot \sum_{\mathbf{k},\lambda} \left(\frac{\hbar\omega_k}{2\varepsilon_0 V} \right)^{1/2} \boldsymbol{\epsilon}_{\mathbf{k},\lambda} (\hat{a}_{\mathbf{k},\lambda} - \hat{a}^\dagger_{\mathbf{k},\lambda}). \tag{10}$$

The permittivity of free space is ε_0, while the polarization vector of the mode $\mathbf{k}$, λ is $\boldsymbol{\epsilon}_{\mathbf{k},\lambda}$. Coupling of the system to the radiation bath causes excitation to the excited electronic manifold, spontaneous emission from these excited states, and the generation of radiation-system Fano coherences. The bath is similarly modeled as a collection of independent harmonic oscillators,[24,33,36] $\hat{H}_B = \sum_{\alpha,m} \hbar\omega_{\alpha m} \hat{b}^\dagger_{\alpha m} \hat{b}_{\alpha m}$, with $\hat{b}^\dagger_{\alpha m}$ and $\hat{b}_{\alpha m}$ being the creation and annihilation operators of mode m and independent bath α. The phonon bath describes the low-frequency vibrational modes of the retinal chromophore, as well as the surrounding protein environment.[24] The phonon bath couples to the operators $\{\hat{q}_\alpha\}$ through the Hamiltonian

$$\hat{H}_{S-B} = \sum_{\alpha,m} \lambda_{\alpha m} (\hat{b}_{\alpha,m} + \hat{b}^\dagger_{\alpha,m}) \hat{q}_\alpha, \tag{11}$$

where the coupling strength $\lambda_{\alpha m}$ is that of the spectral density through[24] $J_\alpha(\omega) = 2\pi \sum_m |\lambda_{\alpha,m}|^2 \delta(\omega - \omega_m)$. In the 2S2M model of

retinal,[33,36] $\hat{q}_\phi = (1-\cos\phi)|\psi_1\rangle\langle\psi_1|$ and $\hat{q}_x = x|\psi_1\rangle\langle\psi_1|$. Coupling to these operators leads to decay of excited state populations into intermediate and product eigenstates,[37] as well as both dephasing and the generation of coherences.[24] We assign an Ohmic form to the spectral density, $J_\alpha(\omega) = \eta_\alpha \omega e^{-\omega/\omega_{c\alpha}}$, with the dimensionless coupling strength η_α and the cutoff frequency $\omega_{c\alpha}$, with the spectral density parameters of Ref. 33.

Under a second-order Born-Markov approximation for both the radiation field and the bath, the system density operator satisfies the master equation

$$\partial_t \hat{\rho}(t) = -\frac{i}{\hbar}[\hat{H}_S, \hat{\rho}(t)] + \sum_{kl} R_{ijkl}\rho_{kl}(t)|i\rangle\langle j|, \tag{12}$$

where $\hat{R}$ is the Redfield tensor and $\hat{H}_S|i\rangle = E_i|i\rangle$ defines the system energy eigenstates.

The form of both the secular and nonsecular Redfield tensors is given in Ref. 25. The effect of solar excitation is contained within the Redfield tensor through the solar thermal occupation number $n(\omega_{ij}) = [\exp[\hbar|\omega_{ij}|/(k_B T_{\text{sun}})] - 1]^{-1}$, where k_B is Boltzmann's constant and $T_{\text{sun}} = 5800$ K is the surface temperature of the sun. To incorporate the natural filtering of incident light, the solar thermal occupation number is multiplied by a factor of C,[28] which is related to the luminance of the light source and is between 10^{-5} and 10^{-9} for typical biological light detection in nature.[24,28]

It is instructive to consider the validity of the Redfield treatment. A perturbative treatment of the system-phonon interaction is expected to be valid when $\eta_\alpha \ll 1$.[36] The parameters of Ref. 33 are $\eta_\phi = 0.05$ and $\eta_x = 0.025$, both of which satisfy the weak-coupling requirement. The only regime in which the Redfield treatment may become inaccurate is strong system-bath coupling (large $\lambda > 5$ discussed later in the text). A perturbative treatment of the system-radiation coupling is valid if $\tau_{\text{rad}} H^2_{\text{S-rad}}/\hbar^2 \ll H_S/\hbar$, where τ_{rad} is the correlation time of the radiation, $H_{S-\text{rad}}$ is the characteristic energy scale of the system-radiation coupling, and H_S is the characteristic energy scale of the system. The free-space spontaneous emission rate is $\gamma \approx 10^9\ \text{s}^{-1}$. The absorption rate is $r = Cn(\omega_0)\gamma$, where $\omega_0 \approx 10^{15}\ \text{s}^{-1}$ is the optical frequency. Since $n(\omega_0) < 1$, we have $r < \gamma$ for $C < 1$. Therefore, $H_{S-\text{rad}}/\hbar$ is of order γ. The coherence time of sunlight is approximately 1 fs[29] so that $\tau_{\text{rad}} H^2_{\text{S-rad}}/\hbar^2 \sim 1000\,\text{s}^{-1}$. For optical excitations, $H_S/\hbar \sim \omega_0$. Hence, the condition $\tau_{\text{rad}} H^2_{\text{S-rad}}/\hbar^2 \ll H_S/\hbar$ is satisfied and a perturbative treatment is valid.

Two alignment terms enter the master equation.[38] The magnitude of solar-induced coherences depends on the alignment between transition dipole matrix elements of the system, through the alignment term $p_{ijkl} = \boldsymbol{\mu}_{ij}\cdot\boldsymbol{\mu}_{kl}/|\mu_{ij}\mu_{kl}|$, with $\hat{\boldsymbol{\mu}}$ being the vectorial dipole operator and matrix elements labeled by the system energy eigenstates. Similarly, the magnitude of bath-induced coherences depends on the alignment of bath operators, through the term $P^\alpha_{ijkl} = q^\alpha_{ij}q^\alpha_{kl}/|q^\alpha_{ij}q^\alpha_{kl}|$. The dipole operator is given by $\hat{\mu} = \mu|\psi_0\rangle\langle\psi_1| + \text{h.c.}$ within the Condon approximation,[24] with the magnitude of the dipole moment taken to be $\mu = 10$ D.[24]

Three different alignment factors for excitation with light are considered below. In the first case, we take all transition dipole moments to be orthogonal, $\boldsymbol{\mu}_{ij}\cdot\boldsymbol{\mu}_{kl} = |\mu_{ij}|^2\delta_{ik}\delta_{jl}$ and refer to this case as "orthogonal dipoles." This choice reproduces the secular equations of motion for the radiation field, wherein rapidly oscillating coherences are decoupled from populations.[38] In the absence of an environment, the populations couple only to each other, no coherences are generated if none are present initially, and any existing coherences simply oscillate and decay. In this case, the solar-induced dynamics are described in terms of absorption and emission rates alone. However, the effect of the environment still allows for the coupling of populations and coherences since $P^\alpha_{ijkl} \neq \delta_{ik}\delta_{jl}$, and hence, the case of orthogonal dipoles still allows for coherence generation. In the second case, we take $\boldsymbol{\mu}_{ij} = \mu_{ij}\boldsymbol{u}$, where $\boldsymbol{u}$ is a unit vector in Euclidean space. Computationally, this corresponds to setting $\hat{\mu} = \mu|\psi_0\rangle\langle\psi_1| + \text{h.c.}$, transforming $\hat{\mu}$ into the energy eigenbasis to obtain μ_{ij}, and then using $\boldsymbol{\mu}_{ij}\cdot\boldsymbol{\mu}_{kl} = \mu_{ij}\mu_{kl}$ for all i, j, k, and l. The transformation of $\hat{\mu}$ into the energy eigenbasis naturally leads to some μ_{ij} which have the same sign as μ_{kl} and others that have opposite signs. Some examples are shown in Fig. 2(a). This case is referred to as "partially aligned dipoles." In the third case, we take $\boldsymbol{\mu}_{ij}\cdot\boldsymbol{\mu}_{kl} = |\mu_{ij}\mu_{kl}|$, which corresponds to parallel alignment of all transition dipole moments [Fig. 2(b)]. This case is referred to as "fully aligned dipoles." As a reference point, we also consider the case that the secular approximation is applied to both the radiation field and the environment, denoted the "full secular approximation." In this case, no coherences are generated if none are present initially. Results below that are obtained "within the secular approximation" correspond to this case in which the secular approximation is applied to *both* the light and the bath.

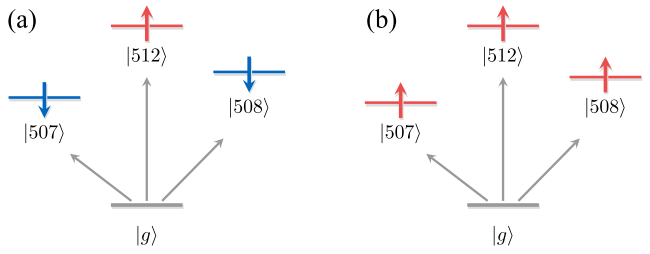

FIG. 2. Diagram of two different dipole alignment schemes in model retinal for sample energy levels. Transition dipole vectors $\boldsymbol{\mu}_{g,i}$ for the bright[24,37] eigenstates $|i\rangle = |507\rangle, |508\rangle, |512\rangle$ are shown with vertical arrows. Straight lines with arrows connecting the ground state $|g\rangle$ to the excited states indicate incoherent excitation. States with antialigned transition dipole vectors are visualized with different colors. (a) Partially aligned dipoles and (b) fully aligned dipoles.

Note that, unlike with partially aligned dipoles, neither orthogonal nor fully aligned dipoles arise from a simple expression for $\hat{\boldsymbol{\mu}}$. Indeed, no $\hat{\boldsymbol{\mu}}$ can yield orthogonal dipoles, for it is not possible for more than three transition dipole moments to be orthogonal to each other. Rather, these cases are simply conceptual examples used to explore the effect of alignment on coherence generation.

III. RESULTS

The dynamics of isomerization under incoherent light were reconstructed for the cases $C = 1$, $C = 10^{-5}$, and $C = 10^{-7}$, with the light turned on instantaneously at $t = 0$. (This turn-on is not expected to alter steady-state results.) Note that $C \sim 10^{-7}$ is most relevant physically for sunlight[28] incident on the eye. In the case

of photocells, C will depend on the photocell design. The dynamics were recreated using three to six progress moments [Eq. (2)] and two to three basis functions [Eq. (1)] depending on the value of C and whether the dynamics were secular or nonsecular. The $\delta\hat{\rho}_n$ matrices each converged within 30–60 min on a laptop with a 2.9 GHz processor. In the same amount of time, the nonsecular master equation for this system could be solved to $t = 1$ ps. The significance of these computational times are discussed further below.

A. Isomerization rates and dynamics

Both the time-dependent dynamics and long time stationary values are of interest. The *trans* probability $\langle \hat{P}_T \rangle$ is shown in Fig. 3(a) with the secular approximation and in Fig. 3(b) with partially aligned dipoles. As seen in Figs. 3(a) and 3(b), the rate at which *cis* is converted to *trans* is mainly determined by C. Indeed, one expects that the isomerization rate should be given by $k_f = rY$, where k_f is the forward isomerization rate, r is the excitation rate, and Y is the quantum yield. The rate of isomerization is seen to be directly proportional to C (and hence to r),[28] as shown in Fig. 4(a). The stationary value of the *trans* probability also decreases as C is reduced. This is because the forward reaction rate decreases, while the thermally induced reverse reaction rate remains constant. In this minimal model for retinal, the inverse of the thermal back-reaction rate is on the order of microseconds, as is evidenced by the microsecond time scale taken to reach the steady state [Figs. 3(a) and 3(b)].

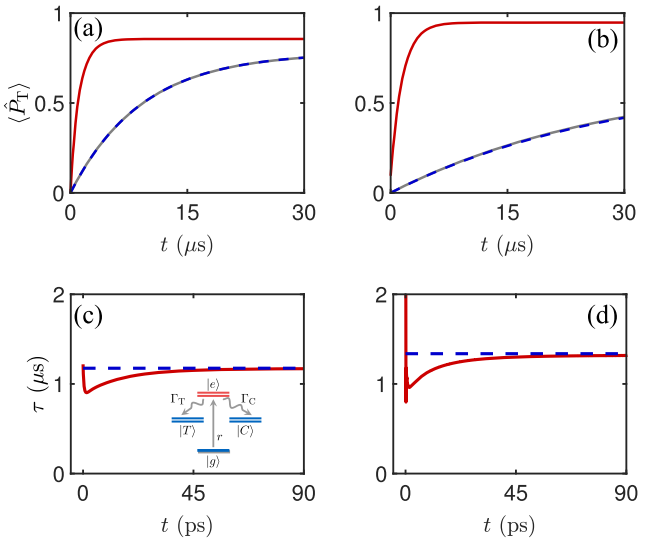

FIG. 3. Isomerization dynamics of model retinal. (a) Reconstructed dynamics of the *trans*-isomer probability for $C = 1$ (solid red), $C = 10^{-5}$ (solid gray; result multiplied by 10^4), and $C = 10^{-7}$ (dashed blue; result multiplied by 10^6) in the full secular approximation. (b) Same as in (a), but with partially aligned dipoles. The results of $C = 10^{-5}$ (solid gray) and $C = 10^{-7}$ (dashed blue) are multiplied by 3×10^3 and 3×10^5, respectively. Note the microsecond abscissa time scale. (c) Comparison of master equation results (solid red) and predicted long time value from the moment method (dashed blue) of the forward reaction time, $\tau \equiv k_f^{-1}$, for $C = 1$ in the full secular approximation. Note the shorter abscissa time scale. [Inset: model energy diagram of the isomerization process under incoherent excitation. Excitation from the ground state $|g\rangle$ populates a set of bright eigenstates $|e\rangle$ (visualized in red), which decay to a set of eigenstates $|C\rangle$ or $|T\rangle$ that are localized in the *cis* and *trans* potential wells, respectively.] (d) Same as in (c), but with partially aligned dipoles.

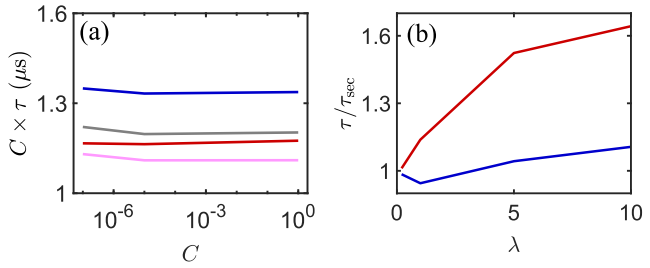

FIG. 4. (a) $C \times \tau$ as a function of C in the full secular approximation (red), with orthogonal dipoles (gray), with partially aligned dipoles (blue), and with fully aligned dipoles (pink) for realistic system-bath coupling. (b) Forward reaction time, normalized to its secular value, for partially aligned dipoles (red) and fully aligned dipoles (blue), as a function of $\lambda = \eta_x/\eta_{x,0} = \eta_\phi/\eta_{\phi,0}$.

The dynamics of $\langle \hat{P}_T \rangle$ differ significantly between the full secular approximation [Fig. 3(a)] and the partially aligned dipole result [Fig. 3(b)]. For example, the rate at which $\langle \hat{P}_T \rangle$ increases in Fig. 3(b) is smaller than in Fig. 3(a), but its stationary value is larger. To explore this result further, consider the energy level schematic given in the inset of Fig. 3(c). Excitation from the ground state $|g\rangle$ populates a set of bright eigenstates $|e\rangle$ with mixed *cis-trans* character. Bath-induced decay transfers population from the bright manifold to a set of eigenstates $|C\rangle$ or $|T\rangle$, which are localized in either the *cis*- or *trans*-potential well, respectively. The probability of *trans* product formation depends on the relative decay rates Γ_T and Γ_C[28] to *trans* and *cis*, as well as the *cis-trans* nature of the different excited states and their relative population.[37] The latter reflects the composition of the system Hamiltonian. The probability of different decay paths, a function of both the excited state distribution and the bath decay rates, determines the probability of ending up in *trans* states. If excitation is the rate-limiting step, then the rate of isomerization should equal rY. The effect of Fano interference is to increase or decrease the quantum yield Y and thus affect the rate of isomerization.

The rate of isomerization in the secular approximation and with partially aligned dipoles is plotted in Figs. 3(c) and 3(d). Note that in Fig. 3, "predicted" refers to the results obtained from progress moments [Eqs. (1) and (3)]. For weak solar-induced excitation, the product population is expected to follow exponential dynamics through

$$\langle \hat{P}_T(t) \rangle = \frac{k_f}{k_f + k_r}\left(1 - e^{-(k_f + k_r)t}\right), \tag{13}$$

where k_r is the reverse reaction rate. Such exponential dynamics are expected to arise after a transient turn-on time t^*, defined through $t_{mic} \ll t^* \ll t_{chem}$, where t_{mic} is the characteristic time scale of the internal system dynamics and t_{chem} is the reaction time scale. The rate $k_f(t)$ is time-dependent before time t^* and can be calculated from $k_f(t) = \partial_t \langle \hat{P}_T(t) \rangle$, which holds for times $t \ll k_f^{-1}$ and $t \ll k_r^{-1}$.

The inverse of the rate is defined as $\tau \equiv k_f^{-1}$. The dynamics for $t < t^*$ are not relevant to the long time dynamics for $t > t^*$. The method that we presented in Ref. 25 allows for the efficient calculation of $k_f(t^*)$ without direct solution of the quantum master equation; the results are shown in Figs. 3(c) and 3(d). Excellent agreement is seen between the long time rate predictions of the reconstructed progress variable (dashed line) and direct numerical simulations of the master equation (red curve). In the nonsecular case, the time-dependent rate $k_f(t < t^*)$ contains oscillations [Fig. 3(d)], which are a result of oscillatory coherences. By $t = t^*$, the oscillations die out and the coherences become stationary. Recent work[23] has shown that these light-induced oscillations disappear as soon as the turn-on of the incoherent light is slow (i.e., when it occurs over a few picoseconds, which is still fast compared to natural millisecond turn-on times).

Note that in this minimal retinal model, the reaction rate and hence the quantum yield, as computed via the master equation, do not stabilize for several tens of picoseconds. The minimum in τ near $t = 2$ ps corresponds to the maximum quantum yield of ≈0.65 observed experimentally and reported theoretically in Ref. 24. The yield then drops over the next tens of picoseconds. It is unclear whether this effect is a result of the model used or is physically relevant, an issue being examined in detail.[27] In either case, the method introduced in Ref. 25 allows us to obtain the long-time reaction rate (dashed line) without propagating the master equation out to $t \approx 80$ ps. Obtaining the detailed short time dynamics via the progress variables would require the Laplace transform approach, noted above.

The inverse forward rate shown in Figs. 3(a) and 3(b) is $\tau = 1.17$ μs in the secular approximation and $\tau = 1.33$ μs with partially aligned dipoles. This 13% increase equivalently corresponds to a 13% decrease in the quantum yield. Evidently in this case, the effect of Fano interference is to decrease the probability of decay through pathways that lead to the *trans* product. Note that the oscillatory coherences generated by the sudden turn-on of radiation have decayed to their stationary or quasistationary values by time $t^* \gg t_{\mathrm{mic}}$. These stationary coherences are expected to have the same value as those generated by slowly turned-on radiation.[23,39] Therefore, the effect of coherence on the reaction rate is not due to the sudden turn-on of radiation.

Before further discussing the effect of Fano interference, note that the method described here is able to obtain the dynamics over a microsecond time scale [Figs. 3(a) and 3(b)] and is clearly more efficient than propagating the full master equation on this time scale. However, if only one rate is needed in the expansion in Eq. (1), then this rate is equal to $k_f + k_r$. The rate k_f can be obtained by propagating the master equation until $k_f(t)$ reaches a constant value. The rate k_r can be obtained through knowledge of $\hat{\rho}_s$. Together, k_f and k_r can then be used to reproduce the entirety of the dynamics. However, in the case considered here, the master equation must be propagated to $t \approx 80$ ps to obtain a converged value for k_f. Propagating the master equation to $t \approx 80$ ps took several days, whereas obtaining τ by calculating the I_n took only 3 h. Thus, our proposed method,[25] used here, can obtain open quantum system dynamics far more quickly than by solving a master equation. The method is particularly relevant for large open quantum systems with multiple time scales, such as a system subject to weak excitation, e.g., due to incoherent light or noise.

B. Fano interference

To better understand the effect of Fano interference, induced by coupling to the bath and/or to the radiation field, we compare the isomerization rates in four different cases: the secular approximation, orthogonal dipoles, partially aligned dipoles, and fully aligned dipoles. As discussed in Sec. II B, "full secular approximation" means here that the secular approximation is applied to both the bath and the light. A secular approximation is not applied to the bath in the last three cases (orthogonal dipoles, partially aligned dipoles, and fully aligned dipoles).

The resultant quantity $C \times \tau$ is shown in Fig. 4(a). Note that if $\tau \propto 1/C$, then $C \times \tau$ vs C should be a flat line. As shown in Fig. 4(a), in all cases, the forward reaction rate is almost exactly proportional to C, independent of the effect of coherences. This is to be expected for weak-field illumination. This would cease to be the case if the excitation time scale were comparable to the time scale of internal dynamics (i.e., the femtosecond to picosecond time scales observed under pulsed laser excitation). The excitation time scale is given by $r^{-1} = C^{-1} r_0^{-1}$, where $r_0^{-1} \approx 1$ μs. If $r^{-1} \approx 1$ ps, then $C = 10^6$. Since $C < 1$ under natural conditions, there are no realistic situations in which $C \times \tau$ should not be constant with respect to C.

The rate is 13% slower with partially aligned dipoles than that with the full secular approximation, 3% slower when the dipoles are orthogonal, and 5% faster when the dipoles are aligned. Note that these latter two cases, in which all dipoles are either orthogonal or fully aligned, were explored in Ref. 24 on a picosecond time scale. These effects are further analyzed by increasing or decreasing the bath coupling strength. Figure 4(b) shows τ normalized to the secular value τ_{sec} for $C = 1$, plotted for different system-bath coupling strengths. In each case, the bath spectral density is modified according to

$$J_\alpha(\omega) = \eta_\alpha \omega e^{-\omega/\omega_{c,\alpha}} \rightarrow J_\alpha(\omega) = \lambda \cdot \eta_\alpha \omega e^{-\omega/\omega_{c,\alpha}}. \tag{14}$$

Figure 4(b) shows an interesting dependence of the reaction rate on the bath coupling for different transition dipole alignments. Light-induced Fano interference can either enhance or diminish the reaction rate in a way that depends strongly on both the dipole alignment and the strength of the system-bath coupling.

It is clear from Fig. 4(b) that this effect results from the complicated interplay of the system bath coupling and the transition dipole alignment. However, several salient features of these results can be observed. The first is that as the bath coupling λ approaches zero, the reaction rate approaches the secular rate, independent of the transition dipole alignment. The reason for this is clear. Previous analytical work has shown that solar excitation generates significant stationary coherences between states that are close in energy and characterized by rapid relaxation.[40] The small energy separation between the states, in conjunction with the significant broadening associated with relaxation, leads to two spectral envelopes that strongly overlap.[41] Thus, the probability of simultaneously exciting each state is significant. The basis for Fano-induced coherence is the simultaneous excitation of two energy eigenstates, which leads to the generation of a coherent superposition.[23,42,43] Bath-induced relaxation thus amplifies the effects of Fano interference by increasing the probability of simultaneous excitation. When relaxation is slow, the absorption line shape of the two states is narrowed. The probability of exciting a state that belongs to both

resonances then decreases, and the effect of solar-induced Fano interference is reduced. Similarly, as the bath coupling strength is reduced, the effect of bath-induced Fano coherences diminishes as well.

The second observation is that the reaction rate becomes smaller for both aligned and partially aligned dipoles for large values of λ. However, the effect is significantly larger for partially aligned dipoles than for aligned dipoles. The third observation is that the full dipole alignment is associated with an increased rate for intermediate values of λ. Taken together, these two observations indicate that in the model being studied here, full dipole alignment enhances the rate, partial alignment reduces the rate, and strong bath coupling also diminishes the rate. Note that since the quantum yield is proportional to the rate, the same trend holds for the quantum yield as well. Hence bath- and solar-induced coherences have a synergistic effect when the transition dipoles are partially aligned, but partially cancel when the dipoles are fully aligned.

These effects can be traced back to the particular form of the bath operators being used. To see why, consider a model V-system with two excited states $|1\rangle$ and $|2\rangle$ separated by energy $\hbar\omega_{21}$ and a ground state $|g\rangle$ (Fig. 5). The energy gap between state $|g\rangle$ and state $|1\rangle$ is on the order of the optical frequency ω_0 such that coherences between the ground state and either excited state vary rapidly and hence can be decoupled from the populations. If each excited eigenstate is excited at rate r, and bath-induced population decay from each state occurs at a rate Γ, then this system is a simplified version of the system shown in the inset of Fig. 3(c). The evolution of the coherence ρ_{12} is obtained from the Bloch-Redfield equation as

$$\dot{\rho}_{12} = pr\rho_{gg} - \frac{1}{2}(pr + P\Gamma)(\rho_{11} + \rho_{22}) - (r + \Gamma)\rho_{12} - i\omega_{12}\rho_{12}. \quad (15)$$

Here, $p = p_{g,e_1,g,e_2}$ is the dipole alignment factor and P quantifies the alignment of the bath operators. For example, if $\Gamma_1 \propto |Q_{1x}|^2$ and $\Gamma_2 \propto |Q_{2y}|^2$, where $\hat{Q}$ is a bath operator that transfers population from $|1\rangle$ to $|x\rangle$ and from $|2\rangle$ to $|y\rangle$, then the factor $P = Q_{1x}Q_{2y}/|Q_{1x}Q_{2y}|$ contains phase information about the transition matrix elements of $\hat{Q}$. Since $\rho_{gg} \gg \rho_{11}, \rho_{22}$ for large Γ, solar excitation is seen to generate coherence through the term $pr\rho_{gg}$, while bath-induced decay generates coherence through the term $-P\Gamma(\rho_{11} + \rho_{22})/2$. Thus, solar excitation generates coherence with the same sign as p, while bath-induced decay generates coherence with the opposite sign of P. Maximal coherence is generated when p and P are of opposite sign, and minimal coherence is generated when p and P are of the same sign. The case of partially aligned dipoles in model retinal indeed corresponds to P and p of opposite sign for many of the bright eigenstates. The case of fully aligned dipoles does not and is thus associated with smaller coherence generation. In this latter case, it is clear from Fig. 4 that solar-induced Fano coherences dominate for moderate system bath coupling, while bath-induced coherences dominate for strong system-bath coupling. The two cancel at a value of λ between 1 and 5.

This analysis indicates that the first observation (regarding the general dependence on λ) is generic, while the second and third observations are specific to the model system being studied. However, an important conclusion that can be drawn from the latter observations is that the correlation between dipole alignment and bath operator alignment is a significant factor in determining the magnitude of interference effects. The case of partial dipole alignment corresponds to a strong negative correlation between the signs of p and P, while full dipole alignment does not. The effects of Fano interference under natural conditions therefore depends strongly on the connection between nuclear coupling to the bath and electronic coupling to the radiation field.

C. Cellular hyperpolarization

While the effects of stationary coherence are interesting, it is clear from Figs. 3(a) and 3(b) that a 13% change due to Fano interference is negligible compared to the variation caused by different excitation intensities. To emphasize this point, we calculate the probability of cellular hyperpolarization as a function of time. The hyperpolarization of a rod cell requires the isomerization of only a few molecules. Following Ref. 28, we calculate this probability as equal to the probability that at least three retinal molecules have undergone isomerization. This is given by $1 - p_0 - p_1 - p_2$, where $p_n = \binom{n}{N} g^n (1-g)^{N-n}$ is the probability that n molecules have undergone isomerization, g is the *trans* probability, and $N = 4 \times 10^9$ is the number of rhodopsin molecules in a rod cell. The results are shown in Fig. 6(a) for $C = 1$, $C = 10^{-5}$, and $C = 10^{-7}$ in the

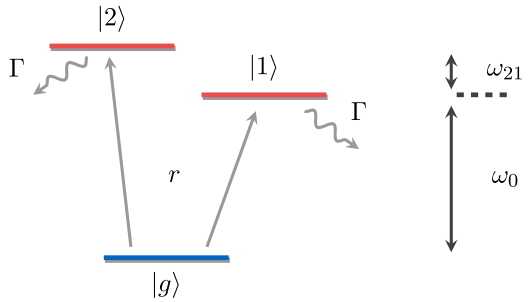

FIG. 5. Energy diagram of a model three-level V-type system used in the analysis of Fig. 4. Excitation is shown with straight gray lines, and relaxation is shown with wavy lines. The excited states are visualized in red and the ground state in blue. The excited states are separated by the energy splitting $\omega_{21} \ll \omega_0$, with ω_0 being the excitation frequency.

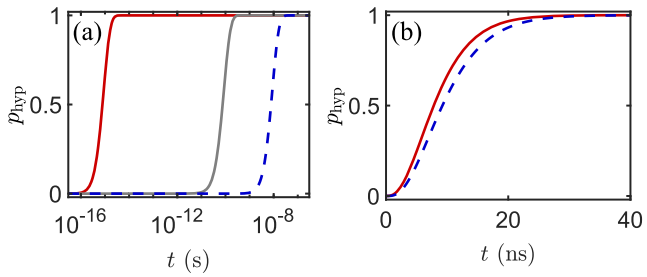

FIG. 6. Probability of hyperpolarization in a single cell as a function of time. (a) In the secular approximation, for $C = 1$ (solid red), $C = 10^{-5}$ (solid gray), and $C = 10^{-7}$ (dashed blue). (b) Probability of hyperpolarization for $C = 10^{-7}$, with partially aligned dipoles (dashed blue) and with the secular approximation (solid red).

secular approximation. A comparison of the probability with the secular approximation and with partially aligned dipoles is shown in Fig. 6(b). Clearly, the probability of hyperpolarization is characterized by a large variation in time scales that is determined by the excitation rate. Nonsecular effects for $C = 10^{-7}$ are seen to be quite small compared to natural variations in intensity. These effects are also minor compared to the effect of adding more rhodopsin molecules.

Although under natural conditions C is many orders of magnitude smaller, it is interesting to observe that for $C = 1$, the probability of hyperpolarization approaches unity on a femtosecond time scale. Here, the dynamics occurring on a femtosecond time scale can still be relevant even if excitation is rate-limiting. This is because the probability of three molecules isomerizing is larger when there are more molecules. With enough molecules, the probability that three molecules isomerize may approach unity at short times, even if the excitation is weak. Note, however, that under natural conditions, this time scale would also depend on the turn-on rate of the light, which here corresponds to sudden turn-on.

IV. CONCLUSION

Utilizing an efficient method[25] to obtain open system dynamics, we have analyzed the *cis-trans* isomerization dynamics of a model of the retinal chromophore in rhodopsin. This approach allowed the efficient evaluation of the effect of coherence on the dynamics on biological time scales. Coherences were shown to lead to a nonnegligible rate decrease of 13% when the light-related transition dipoles are partially aligned and a rate enhancement of 5% when they are fully aligned. Increasing the coupling between the system and the protein environment can either enhance or reduce the effect of solar-induced Fano interference on the reaction rate. These results indicate that model retinal isomerization under incoherent illumination can be moderately impacted by the effects of quantum coherence. However, the main determinant of the biologically relevant time scales, such as the time taken for cellular hyperpolarization, is found to be the intensity of radiation. The robustness of the light-sensing process to changes in the solar intensity is a result of the efficiency of the process and the large number of retinal molecules in a cell.

ACKNOWLEDGMENTS

The authors thank Cyrille Lavigne for enlightening discussions. This work was supported by the U.S. Air Force Office of Scientific Research (AFOSR) under Contract No. FA9550-17-1-0310.

REFERENCES

[1] G. Panitchayangkoon, D. Hayes, K. A. Fransted, J. R. Caram, E. Harel, J. Wen, R. E. Blankenship, and G. S. Engel, Proc. Natl. Acad. Sci. U. S. A. **107**, 12766 (2010).
[2] E. Collini, C. Y. Wong, K. E. Wilk, P. M. G. Curmi, P. Brumer, and G. D. Scholes, Nature **463**, 644 (2010).
[3] G. S. Engel, T. R. Calhoun, E. L. Read, T.-K. Ahn, T. Mančal, Y.-C. Cheng, R. E. Blankenship, and G. R. Fleming, Nature **446**, 782 (2007).
[4] A. W. Chin, A. Datta, F. Caruso, S. F. Huelga, and M. B. Plenio, New J. Phys. **12**, 065002 (2010).
[5] S. Lloyd and M. Mohseni, New J. Phys. **12**, 075020 (2010).
[6] H. Lee, Y.-C. Cheng, and G. R. Fleming, Science **316**, 1462–1465 (2007).
[7] Q. Wang, R. W. Schoenlein, L. A. Peteanu, R. A. Mathies, and C. V. Shank, Science **266**, 422 (1994).
[8] W. Bialek, *Biophysics: Searching for Principles* (Princeton University Press, 2012).
[9] P. J. M. Johnson, A. Halpin, T. Morizumi, V. I. Prokhorenko, O. P. Ernst, and R. J. D. Miller, Nat. Chem. **7**, 980 (2015).
[10] K. Palczewski, J. Biol. Chem. **287**, 1612 (2012).
[11] J. L. Spudich and K.-H. Jung, *Handbook of Photosensory Receptors* (Wiley-VCH, 2005).
[12] K. Schulten and P. Tavan, Nature **272**, 85 (1978).
[13] A. A. Svidzinsky, K. E. Dorfman, and M. O. Scully, Phys. Rev. A **84**, 053818 (2011).
[14] M. O. Scully, K. R. Chapin, K. E. Dorfman, M. B. Kim, and A. Svidzinsky, Proc. Natl. Acad. Sci. U. S. A. **108**, 15097 (2011).
[15] K. E. Dorfman, D. V. Voronine, S. Mukamel, and M. O. Scully, Proc. Natl. Acad. Sci. U. S. A. **110**, 2746 (2013).
[16] F. Rieke and D. A. Baylor, Rev. Mod. Phys. **70**, 1027 (1998).
[17] N. Sim, M. F. Cheng, D. Bessarab, C. M. Jones, and L. A. Krivitsky, Phys. Rev. Lett. **109**, 113601 (2012).
[18] N. M. Phan, M. F. Cheng, D. A. Bessarab, and L. A. Krivitsky, Phys. Rev. Lett. **112**, 213601 (2014).
[19] X.-P. Jiang and P. Brumer, J. Chem. Phys. **94**, 5833 (1991).
[20] P. Brumer and M. Shapiro, Proc. Natl. Acad. Sci. U. S. A. **109**, 19575 (2012).
[21] P. Brumer, J. Phys. Chem. Lett. **9**, 2946 (2018).
[22] T. Tscherbul and P. Brumer, J. Chem. Phys. **148**, 124114 (2018).
[23] A. Dodin and P. Brumer, J. Chem. Phys. **150**, 184304 (2019).
[24] T. V. Tscherbul and P. Brumer, Phys. Chem. Chem. Phys. **17**, 30904 (2015).
[25] S. Axelrod and P. Brumer, J. Chem. Phys. **149**, 114104 (2018).
[26] S. Hahn and G. Stock, J. Phys. Chem. B **104**, 1146 (2000).
[27] C. Chuang and P. Brumer, "Improved retinal model under natural incoherent excitation" (unpublished).
[28] K. Hoki and P. Brumer, Procedia Chem. **3**, 122 (2011).
[29] H. P. Breuer and F. Petruccione, *The Theory of Open Quantum Systems* (Oxford University Press, 2002).
[30] S. Nakajima, Prog. Theor. Phys. **20**, 948 (1958).
[31] R. Zwanzig, J. Chem. Phys. **33**, 1338 (1960).
[32] P. Hänggi, P. Talkner, and M. Borkovec, Rev. Mod. Phys. **62**, 251 (1990).
[33] B. Balzer, S. Hahn, and G. Stock, Chem. Phys. Lett. **379**, 351 (2003).
[34] D. Polli, P. Altoè, O. Weingart, K. M. Spillane, C. Manzoni, D. Brida, G. Tomasello, G. Orlandi, P. Kukura, R. A. Mathies *et al.*, Nature **467**, 440 (2010).
[35] M. O. Scully and M. S. Zubairy, *Quantum Optics* (Cambridge University Press, 1997).
[36] B. Balzer and G. Stock, Chem. Phys. **310**, 33 (2005).
[37] T. V. Tscherbul and P. Brumer, J. Phys. Chem. A **118**, 3100 (2014).
[38] T. V. Tscherbul and P. Brumer, J. Chem. Phys. **142**, 104107 (2015).
[39] T. Grinev and P. Brumer, J. Chem. Phys. **143**, 244313 (2015).
[40] T. Mančal and L. Valkunas, New J. Phys. **12**, 065044 (2010).
[41] I. Kassal, J. Yuen-Zhou, and S. Rahimi-Keshari, J. Phys. Chem. Lett. **4**, 362 (2013).
[42] A. Dodin, T. V. Tscherbul, and P. Brumer, J. Chem. Phys. **145**, 244313 (2016).
[43] A. Dodin, T. V. Tscherbul, and P. Brumer, J. Chem. Phys. **144**, 244108 (2016).